Journal of Thrombosis and Haemostasis, **8**: 1030–1036 DOI: 10.1111/j.1538-7836.2010.03745.x

IN FOCUS

The mechanical properties of single fibrin fibers

W. LIU,[1] C. R. CARLISLE,[1] E. A. SPARKS and M. GUTHOLD
Department of Physics, Wake Forest University, Winston-Salem, NC, USA

To cite this article: Liu W, Carlisle CR, Sparks EA, Guthold M. The mechanical properties of single fibrin fibers. *J Thromb Haemost* 2010; **8:** 1030–6.

See also Weisel JW. Biomechanics in hemostasis and thrombosis. This issue, pp 1027–9. Carlisle CR, Sparks EA, Der Loughian C, Guthold M. Strength and failure of fibrin fiber branchpoints. This issue, pp 1135–8.

Summary. *Background:* Blood clots perform the mechanical task of stemming the flow of blood. *Objectives:* To advance understanding and realistic modeling of blood clot behavior we determined the mechanical properties of the major structural component of blood clots, fibrin fibers. *Methods:* We used a combined atomic force microscopy (AFM)/fluorescence microscopy technique to determine key mechanical properties of single crosslinked and uncrosslinked fibrin fibers. *Results and conclusions:* Overall, full crosslinking renders fibers less extensible, stiffer, and less elastic than their uncrosslinked counterparts. All fibers showed stress relaxation behavior (time-dependent weakening) with a fast and a slow relaxation time, 2 and 52 s. In detail, crosslinked and uncrosslinked fibrin fibers can be stretched to 2.5 and 3.3 times their original length before rupturing. Crosslinking increased the stiffness of fibers by a factor of 2, as the total elastic modulus, E_0, increased from 3.9 to 8.0 MPa and the relaxed, elastic modulus, E_∞, increased from 1.9 to 4.0 MPa upon crosslinking. Moreover, fibers stiffened with increasing strain (strain hardening), as E_0 increased by a factor of 1.9 (crosslinked) and 3.0 (uncrosslinked) at strains $\varepsilon > 110\%$. At low strains, the portion of dissipated energy per stretch cycle was small ($< 10\%$) for uncrosslinked fibers, but significant (approximately 40%) for crosslinked fibers. At strains $> 100\%$, all fiber types dissipated about 70% of the input energy. We propose a molecular model to explain our data. Our single fiber data can now also be used to construct a realistic, mechanical model of a fibrin network.

Keywords: atomic force microscopy (AFM), fluorescence microscopy, mechanical properties, single fibrin fibers.

Correspondence: Martin Guthold, Department of Physics, 7507 Reynolda Station, Wake Forest University, Winston-Salem, NC 27109, USA.
Tel.: +1 336 758 4977 ; fax: +1 336 758 6142.
E-mail: gutholdm@wfu.edu

[1]These authors contributed equally to this manuscript.

Received 30 July 2009, accepted 7 January 2010

Introduction

Blood clots have the essential mechanical task of stemming the flow of blood, and for the past six decades there has been continuing interest in resolving the mechanical properties of clots and their constituents [1]. The importance of the mechanical properties of a clot is underscored by the fact that they can be related to clotting disorders and disease [2,3]. Properties of the whole, macroscopic clot can be determined via rheometry [3–6]. Moreover, single molecule experiments [7] and the known X-ray structure of fibrinogen provide molecular information [8]. A combination of rheometry, electron microscopy and small angle X-ray diffraction, has recently also been used to investigate the multiscale mechanical behavior of fibrin polymers [6], suggesting that protein unfolding plays an important role at the molecular scale, while fiber stretching and fiber alignment play key roles at the meso- and macroscopic scales. However, single fiber properties that connect underlying molecular mechanisms and macroscopic mechanical properties of a clot, have only recently started to emerge, and their understanding remains far from complete [1]. This single fiber knowledge is critical for constructing mechanical models of clots and, thus, deeper understanding of clot behavior [1,6].

Blood clots are formed when soluble fibrinogen is converted to fibrin monomers that polymerize to form a network of fibrin fibers. The network is further stabilized by the formation of covalent bonds (crosslinks) between specific glutamine and lysine residues of the fibrin monomers [3]. It is this branched network of fibrin fibers that mostly determines the mechanical properties of a clot. Generally, the mechanical properties of such a network depend on three network properties [9,10]: (i) the network architecture, which describes the overall structural composition of the network; (ii) the mechanical properties of the individual fibers that comprise the network; and (iii) the properties of the joints between fibers. The architecture of the fibrin network may be determined from microscopy images [3]. However, beside the extensibility and elastic limit [11], the elastic modulus for small strains [12] and the rupture force of dried fibrin fibers [13], the mechanical properties of single fibrin fibers are unknown. Yet, exactly this knowledge on the single fiber level is needed to construct and test mechanical models of clots and, thus, advance our understanding of clot mechanical

behavior [1,6,9,10]. The mechanical properties of fibrin fibers are among the crucial factors that determine if a clot will deform, rupture or embolize. Considering the fact that blood clots can embolize, it is clear that physiological blood flow can create a large enough force to deform and rupture fibrin fibers.

We have developed a combined AFM/fluorescence microscopy technique to determine the mechanical properties of individual nanoscopic fibers [14]. We have collected stress–strain (force-extension) curves over the entire, extraordinarily large extensibility range of crosslinked and uncrosslinked fibrin fibers and report their distinct mechanical behavior. We have determined the (i) extensibility (stretchability), (ii) elasticity, (iii) strain hardening behavior (stiffening with increased stretching), (iv) energetic behavior (dissipated and stored energy), (v) total and (vi) relaxed elastic modulus (viscoelastic stiffness), and (vii) stress relaxation behavior (time-dependent behavior). We propose a molecular model, based on two major secondary structure transformations and an extension of the interacting αC regions of the fibrin monomer, to explain the observed mechanical behavior.

Materials and methods

Fibrin fiber formation

Uncrosslinked and crosslinked fluorescently labeled fibrin fibers were formed on a striated substrate made from cured optical adhesive (Data S1, Details, supplement). All experiments were carried out in 'fibrin buffer' (140 mM NaCl, 10 mM Hepes, 5 mM $CaCl_2$, pH 7.4). For each experiment, two samples were prepared in parallel. One sample was used for the AFM manipulation experiments, the other for SDS PAGE. Crosslinked samples showed complete γ–γ and α–α crosslinking (≧90%), while the samples without added factor XIII showed no crosslinking.

Manipulation of fibers

The mechanical manipulations of fibrin fibers were performed with a combined AFM/optical microscope instrument (Data S1, Details, supplement). The schematic set-up is shown in Fig. 1(A,B). The instrument is based on a Zeiss (Zeiss, Thornwood NY, USA) inverted optical microscope, a Hamamatsu, high sensitivity camera (Hamamatsu Photonics KK, Hamamatsu, Japan) and a Topometrix Explorer AFM (Veeco Instruments, Woodbury, NY, USA). The microscope stage was designed so that the AFM tip, fiber sample and objective lens can move with respect to each other, which allows alignment of the fiber with the AFM tip and objective lens. The AFM manipulation experiments were done with a nanoManipulator, a software program that interfaces the AFM with a force feedback stylus and a graphics computer [15]. The nanoManipulator provides control over the *x*-, *y*- and *z*-movement of the AFM tip. The AFM tip is used to stretch the fibrin fibers that are suspended across 12 μm wide channels in the striated, transparent substrate. The fluorescence microscope, situated underneath the substrate, is used to collect movies of this stretching process (Movies S1 and S2, see supplement). The extension of the fiber was determined by fluorescence microscopy and calculation using the distance traveled by the AFM tip (Fig. 1B). The applied force was determined from the twist of the cantilever. The force measurements were calibrated via the Sader method [16] and the Liu method [17].

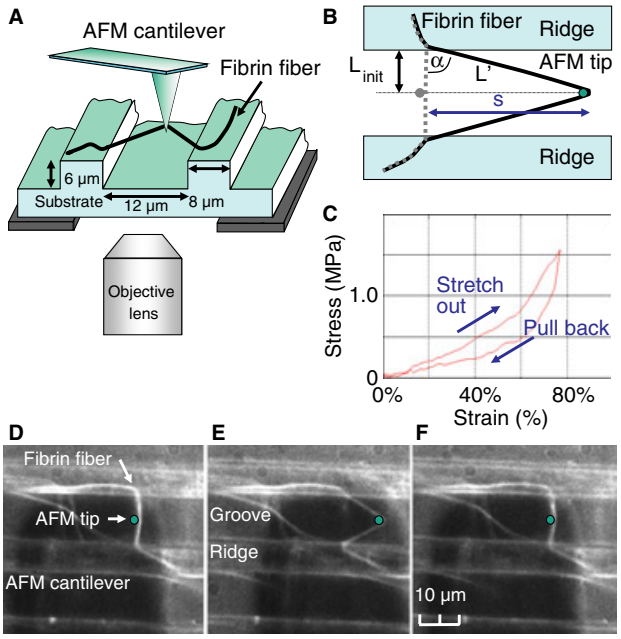

Fig. 1. Experimental set-up. (A) Schematic of atomic force microscope (AFM) sitting on top of the inverted optical microscope. (B) Top view of stretched fiber. The initial and stretched states are in dotted gray and solid black, respectively. (C) Typical fibrin fiber stress–strain curve. (D–F) Fluorescence microscopy movie frames of a stretching experiment. The fiber is anchored on two ridges (brighter, horizontal, 8 μm wide bars) and suspended over a groove (darker, horizontal, 12 μm wide bars); the AFM cantilever appears as a 35 μm wide, dark rectangle; the AFM tip is indicated as a green dot.

Results

Stress–strain curves

For manipulations, we selected single fibers bridging the grooves in a straight line approximately perpendicular to the ridge edge. We have found that most fibers are well anchored on the ridges of the striated substrate, even at extreme fiber extensions. We excluded fibers that slipped on the ridges from our analysis. This experimental design yields a well-defined geometry to determine the mechanical properties of fibrin fibers (Fig. 1A,B).

The mechanical properties of polymers are generally determined via stress–strain (force-extension) curves in which stress, σ, is plotted as a function of strain (deformation), ε, under a variety of conditions. For longitudinal stretching experiments, as done here, stress is defined as F/A, where F is the applied force and A is the *initial* cross-sectional area of the stretched polymer. This is the definition of the commonly used *engineering stress*, which uses the initial cross-section and does

not consider how the cross-sectional area changes as ε increases. Engineering stress gives a lower limit for the stress applied to the polymer, because the cross-sectional area most likely decreases as the fiber is stretched. Strain is defined as $\Delta L/L_{init}$, or $(\Delta L/L_{init})\cdot 100\%$, where ΔL is the change in length and L_{init} is the initial length. A typical stress–strain curve of a fibrin fiber being stretched to 1.75 times its initial length ($\varepsilon = 0.75\%$ or 75%) is shown in Fig. 1(C). The forward and return paths do not overlap; this means that energy (proportional to area under curves) is lost in this stretching cycle. However, although energy is lost, there is no permanent lengthening of the fiber (σ on return path does not reach 0 until $\varepsilon = 0$). The energy loss is due to the viscous properties of fibrin fibers and it is an indication that fibrin fibers are *viscoelastic* polymers. The slope of this curve corresponds to the stiffness (modulus) of the fiber, here about 1.3 MPa. However, it is apparent that such a simple analysis of just the slope misses some key properties of the fiber, such as its viscoelasticity, energy loss, and stiffening with increasing strain. In our experiments we analyzed basic and viscoelastic mechanical properties. A typical movie sequence of a fibrin fiber stretching experiment is shown in Fig. 1(D–F) (Movies S1 and S2 and Data S2, Additional data, see supplement).

Fibrin extensibility and elastic limit

Previously, fibrin fiber extensibility, ε_{max}, defined as the strain (extension) at which fibers rupture, was determined to be 333% and 226% for partially crosslinked and uncrosslinked fibrin fibers, respectively [11]. The elastic limit, $\varepsilon_{elastic}$, defined as the largest strain to which fibers can be stretched and recover to their original length without visible permanent deformation, was previously determined to be 180% and 120% for partially crosslinked and uncrosslinked fibrin fibers [11]. It is important to note that the fibers in this previous study were only partially crosslinked. Here, we determined the extensibility and elastic limit of *fully* crosslinked fibrin fibers. ε_{max} was 147%, which is lower than both partially crosslinked and uncrosslinked fibrin fibers. We found the elastic limit of fully crosslinked fibers to be ≤ 50% strain. For a few manipulations, the elastic limit was 50% strain; however, many fibers showed permanent deformation at strains as low as 10% (see Movies S1 and S2 in supplement). All mechanical properties of crosslinked and uncrosslinked fibers are summarized in Table 1; Table S1 in the supplement also includes all the data for *partially* crosslinked fibers.

Strain hardening

Strain hardening refers to the phenomenon when the elastic modulus (stiffness, slope of the stress–strain curve) increases (hardens) with increasing strain. We observed strain hardening, occurring at approximately 100% strain, for all fibrin fibers. However, crosslinked and uncrosslinked fibers do display several differences: uncrosslinked fibers are initially softer; they show larger extensibilities and significant strain hardening.

Table 1 Mechanical properties of fibrin fibers; the average values and standard errors are listed (see supplement for partially crosslinked fibers and statistics). ε_{max}, extensibility; $\varepsilon_{elastic}$, elastic limit; E_0, total elastic modulus; E_∞, relaxed elastic modulus; τ_1, fast relaxation time; τ_2, slow relaxation time; *h*, strain hardening factor (ratio of the total modulus at high strains (above 110%) to the total modulus at low strains (0%–80%)). Thus, the total elastic modulus for uncrosslinked fibers has a value of 3.9 MPa at low strains and 11.7 MPa at high strains. Crosslinked fibers did not show consistent strain hardening. E_{loss}, percentage energy loss per stretch cycle (energy loss at low strains is close to 0% for uncrosslinked, and ≤ 40% for crosslinked fibers)

Fiber type	Crosslinked	Uncrosslinked
ε_{max}	147% ± 5%	226% ± 8.7%*
$\varepsilon_{elastic}$	≤ 50%	120%*
E_0 (MPa)	8.0 ± 1.0	3.9 ± 0.6
E_∞ (MPa)	4.0 ± 0.6	1.9 ± 0.3
τ_1 (s)	2.1 ± 0.2	3.6 ± 1.3
τ_2 (s)	49 ± 4	57 ± 8
h	1.9 ± 0.3	3.0 ± 0.3
E_{loss}	≤ 40%–70%	0%–70%

*Values from [11].

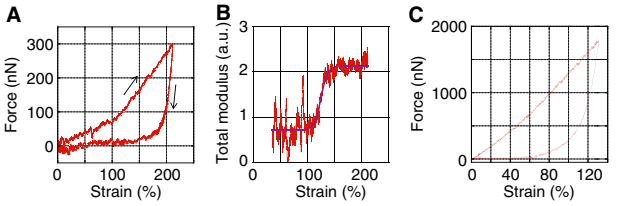

Fig. 2. Strain hardening. (A) Stress–strain curve of an uncrosslinked fibrin fiber. (B) The total elastic modulus, E_0 [slope of forward curve in (A)] as a function of strain. (C) Stress–strain curve for a crosslinked fibrin fiber.

Crosslinked fibers are initially stiffer, show less extensibility and show less pronounced strain hardening. In Fig. 2(A), a stress–strain curve of an uncrosslinked fibrin fiber is plotted. In Fig. 2(B) the total elastic modulus, E_0, which is the *slope* of the forward stress–strain curve in Fig. 2(A), is plotted as a function of strain. The curve displays a distinct sigmoidal shape; the total elastic modulus is relatively constant for the first 100% of strain; it then increases by a factor of about 3 and then remains at this higher value until the fiber ruptures. The strain hardening factor, *h*, that is the average ratio of the total elastic modulus at large strain (at $\varepsilon > 110\%$) to that at small strain ($\varepsilon < 80\%$) is listed in Table 1. On average, uncrosslinked fibers harden by a factor of 3.0 ($P \le 0.0008$). A strain hardening factor of 1.9 ($P \le 0.049$) was determined for crosslinked fibers. However, while crosslinked fibers did show significant strain hardening, as indicated by *t*-test analysis, hardening occurred with less consistency. Figure 2(C) shows a crosslinked fibrin fiber, stretched to 130%, which does not show strain hardening.

Stored and dissipated energy per stretch cycle

As seen in Fig. 1(C), not all of the energy put into stretching a fibrin fiber (area under forward stress–strain curve) is stored. A fraction of this energy is lost (dissipated) due to viscous

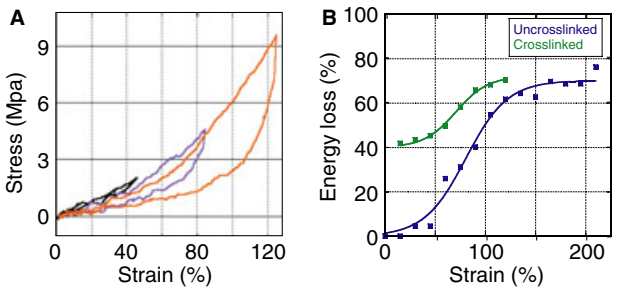

Fig. 3. Energy loss. (A) Stress–strain curve for three consecutive pulls of uncrosslinked fiber with strains of 48%, 85% and 125%. The energy loss corresponds to the area inscribed in a cyclical stress–strain curve. (B) Ratio (percentage) of energy lost vs. total energy for crosslinked fibers (gray) and uncrosslinked fibers (black). Sigmoidal fitting curves of the form $R = R_1 + \frac{R_2 - R_1}{1+e^{\frac{\varepsilon - \varepsilon_0}{\varepsilon^*}}}$, were used to fit the data. R_1 is the initial value, R_2 is the final value, ε_0 is the strain at the inflection point.

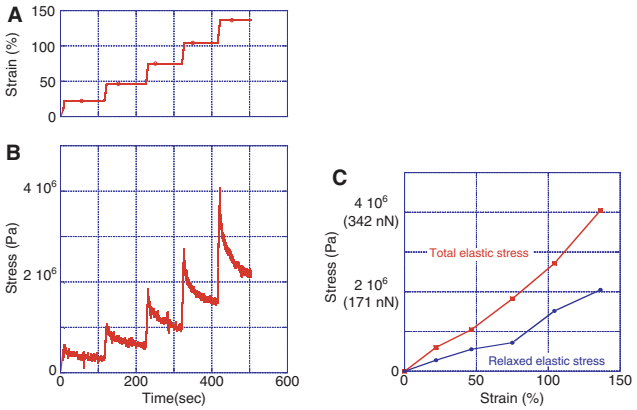

Fig. 4. Incremental stress–strain curves. (A) Strain vs. time and (B) stress vs. time for an incremental stress–strain curve of a fibrin fiber. The *x*-axis (time) is the same for (A) and (B). The strain is held constant at 23%, 46%, 75%, 104% and 138% for about 120 s. The stress decays exponentially at each strain value. (C) Total stress (squares) and relaxed stress (dots) vs. strain as obtained from the data in (A) and (B).

processes. The dissipated energy is proportional to the area inscribed by the forward and backward curves. We have determined the amount of dissipated energy per stretch cycle as a function of strain (Fig. 3). Uncrosslinked fibers show little energy loss at low strains and 70% energy loss at high strains. Crosslinked fibers already show significant energy loss at low strains.

Figure 3(A) shows three pulling cycles on the same uncrosslinked fibrin fiber with strains of 48%, 85% and 125%, respectively. It can be seen that the fiber dissipated almost no energy (all energy is stored) in the first pull ($\varepsilon = 48\%$), as the area between the forward and backward curve is very small. However, for larger strains ($\varepsilon = 85\%$ and $\varepsilon = 125\%$) a significant fraction (28% and 43%, respectively) of the energy is dissipated. It should be noted that even though large amounts of energy are dissipated, uncrosslinked fibers still return to their original length, meaning that they did *not* permanently lengthen, at strains $< 120\%$ [11].

In Fig. 3(B), the ratio (percentage) of dissipated energy to the total energy is plotted as a function of strain. The graph for uncrosslinked fibers shows a clear sigmoidal shape. The energy loss at low strains is very small; it then increases significantly at strains between 50% and 100% and remains at a constant, higher energy loss level of around 70% for larger strains.

Conversely, crosslinked fibers showed significant energy loss at low strains (43% energy loss for small strains of $\varepsilon < 40\%$). At larger strains ($\varepsilon > 40\%$), the energy loss increased to a plateau of 70% at 100% strain. This increased energy loss (at low strains) for crosslinked fibers is consistent with the notion that crosslinked fibers undergo permanent deformation at much lower strains ($\varepsilon_{elastic} < 50\%$) than uncrosslinked fibers.

Total and relaxed elastic moduli (fiber stiffness)

Both uncrosslinked and crosslinked fibrin fibers show clear viscoelastic (time-dependent) behavior. We also found that crosslinking increases the stiffness (total and relaxed elastic modulus) by a factor of 2.

Incremental stress–strain curves [18] are a technique to separate the elastic (energy stored) and viscous (energy lost) components in viscoelastic materials (Fig. 4). In this technique, the fiber is stretched to a certain strain, where it is held constant for some time. Due to viscous processes, the fiber relaxes; that is, the force (stress) to hold it at that strain decreases. Subsequently, the fiber is stretched by another increment and held at constant strain. Again, the fiber relaxes and the stress decreases. This incremental straining is repeated several times. Figure 4(A) shows the strain vs. time curve of a fibrin fiber; the fiber was incrementally stretched to 23%, 46%, 75%, 104% and 138% strain and held constant at those strains for about 120 s. Figure 4(B) shows the corresponding stress vs. time curve of this fiber and it is readily apparent that the fiber relaxes (stress decreases) at each constant strain value. The *x*-axis (time) in Fig. 4(A,B) is the same. The stress does not decay to zero, but to a constant value at each strain. When plotting each of the peak stress values vs. strain and the relaxed stress values vs. strain, the stress–strain curves in Fig. 4(C) are obtained. The relaxed stress values, σ_∞ for $t \to \infty$, were obtained by fitting two exponentials (Data S1, Details, see supplement). The slope of the higher curve in Figure 4(C) is the total elastic modulus, E_0, obtained before relaxation, and the slope of the lower curve is the relaxed, elastic modulus, E_∞, of fibrin fibers, obtained for $t \to \infty$. For crosslinked fibers, E_0 was 8.0 MPa, and E_∞ was 4.0 MPa. For uncrosslinked fibers, E_0 was 3.9 MPa and E_∞ was 1.9 MPa. Somewhat simplistically speaking, E_0 corresponds to the stiffness of the fibers when they are pulled fast, and E_∞ when they are pulled slowly. For comparison, other materials with stiffness in the MPa range are elastin fibers, spider silk, or a soft rubber band [19].

Stress relaxation

Stress relaxation, as seen in Fig. 4(B), is indicative of viscous (time-dependent) processes [5]. Stress relaxation curves are

usually fitted with one or more exponential functions yielding stress relaxation times. We have done an analysis of the stress relaxation behavior of fibrin fibers using a generalized Kelvin model (Data S2, see supplement). Both crosslinked and uncrosslinked fibers show two stress relaxation rates; a fast (2–4 s) and a slow relaxation rate (49–57 s). These two rates are indicative of two distinct molecular relaxation processes, such as a molecular unfolding or transformation event, occurring with these time scales.

Discussion

We have investigated the mechanical properties of single crosslinked and uncrosslinked fibrin fibers. All our findings are summarized in Table 1 (and Table S1, which includes the data for partially crosslinked fibers).

Our values for the total elastic modulus, E_0, for uncrosslinked and crosslinked fibers (3.9 and 8.0 MPa) agree to within a factor of 2 with the small strain values obtained by Collet *et al.* [12] (1.7 and 14.5 MPa) as determined by laser tweezers. The differences may be explained by the different experimental set-ups and inherent, instrumentation-related errors.

The force *per fibrin monomer* can also be estimated from our data and compared with single protein unfolding experiments (Data S2, Calculations, see supplement). From our data, the force per monomer at 100% strain is about 140 pN, which is consistent with the 100 pN force to stretch a single fibrin monomer by 100% found by Brown *et al.* [7]. From our data, the rupture force per monomer is about 280 pN, which is similar to the 260 pN (2.130 pN) required to rupture the two A:a interactions between half-staggered monomers within a protofibril [20]. Interestingly, these forces are smaller than some protein unfolding forces [21], suggesting that some regions of the fibrin monomer may unfold *before* the fiber ruptures.

The energy per monomer required to rupture the fiber, as obtained from the area under our stress–strain curves (2400 kJ mol^{-1}), is of the same order of magnitude as the melting enthalpy of fibrin molecules (4650 kJ mol^{-1}) [22] (Data S2, Calculations, see supplement), again indicating that fibrin may melt (denature), before the fiber ruptures.

Crosslinking had a significant and intriguing effect on several mechanical properties, and no effect on other properties. Uncrosslinked fibrin fibers are very extensible, are elastic at high strains, are relatively soft, show strain hardening by a factor of 3.0, and a sigmoidal energy loss curve going from 0% loss at low strains to 70% loss at high strains. Complete crosslinking makes fibers stiffer, less extensible, and more susceptible to plastic deformation at a lower strain, and increases the low-strain energy loss. Being already stiffer, crosslinked fibrin fibers did not show the same amount of strain hardening and often did not extend to strains at which strain hardening would have occurred. γ–γ crosslinks form between two reciprocal sites on the abutting γ-nodules of aligned fibrin monomers within a protofibril, and they are thought to be oriented along the longitudinal fiber axis. α–α crosslinks form between numerous sites on the extensive, flexible and partially unstructured αC regions (α221–610), and due to the length of this domain they may be oriented in the lateral (radial direction) and longitudinal direction. In previous experiments, partially crosslinked fibrin showed the largest extensibility (330%) [11]. Thus, crosslinking seems to have a bell-shaped effect on extensibility; from ε_{max} = 230% (uncrosslinked) to ε_{max} = 330% (partial crosslinking) to ε_{max} = 150% (fully crosslinked). Full crosslinking appears to have a restricting effect on previously mobile regions (e.g. the αC regions); it may prevent unfolding of domains and/or it might tighten the fibrin monomer and protofibril interactions.

Clot rheology studies on *whole clots* showed that crosslinking induces a 2–3.5-fold increase of rigidity [3,23,24] of the whole clot, which is similar to the 2-fold increase in E_0 of single fibers we observed.

To explain the observed mechanical behavior of fibrin fibers, we propose a model with the following three molecular mechanisms (Fig. 5). The mechanisms may occur in parallel as the fibers are stretched. (i) α-helix to β-strand conversion of the two coiled coils of the fibrin monomer. This conversion can account for 90–100% strain [7,19]. (ii) Deformation or partial unfolding of the γ-nodule of the fibrin monomer. This conversion may account for an additional 220% strain [19]. These two mechanisms may dynamically fluctuate between

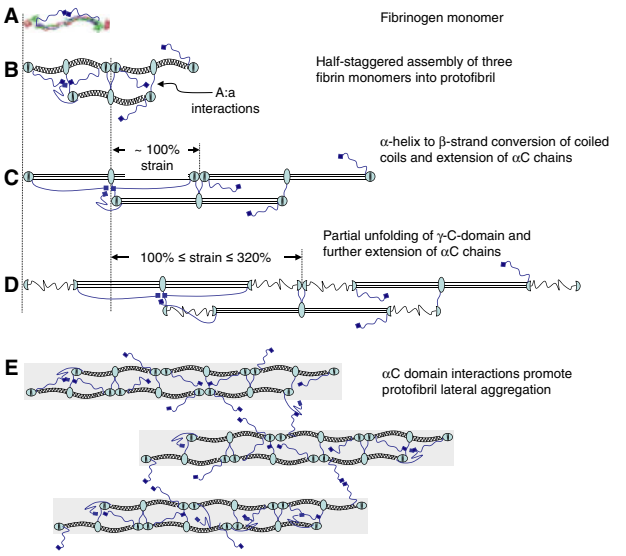

Fig. 5. Model for fibrin fiber extensions. (A) Crystal structure of fibrinogen [8]; the Aα chains, Bβ chains and γ chains are in blue, red and green, respectively (please see the online version of this article for figure colors). A cartoon depiction of the flexible αC region is added to the crystal structure as a blue line and blue square; αC regions may interact with each other within a protofibril, and across protofibrils. (B) Schematic model of half-staggered assembly of three fibrin monomers into protofibril (β-nodule is no longer depicted). (C) An α-helix to β-strand conversion of the coiled coil and a slight straightening and alignment of the molecules could accommodate approximately 100% strain. Some of the αC regions are also extended at this point. (D) Higher strains, up to 320% could be accommodated by a partial unfolding of the globular γ-nodule; 230% strain is depicted. Further extension of the αC region could occur. (E) Interactions between αC regions promote lateral aggregation of protofibrils; they can be elastically extended.

each other (inter-convert). (iii) Interaction and extension of the long, flexible and partially unstructured αC region. The αC region (α221–610) consists of an unstructured connector region (α221–391), and the terminal domain (α392–610). There is evidence that interactions between the αC regions may play a role in fiber assembly, especially lateral aggregation [25–27]. It was also found that a shorter length of the αC connector (in different species) correlates with a lower extensibility of fibers [26].

This model may explain several experimental observations. (i) Two relaxation rates. If viscoelastic mechanisms 1 and 2 occur at different rates and if they are inter-convertible, two different relaxation rates would be observed. For example, the α-helical conversion may happen at a faster rate (and lower force) and the unfolding of the γC region may happen at a slower rate (and higher force). (ii) Strain hardening occurring at about 100% strain. The faster α-helical conversion provides 100% strain, after that γ-nodule unfolding becomes dominant. (iii) The dramatic and sigmoidal increase in energy loss with increasing strain. At larger strains the γ-nodule unfolds more extensively, which may not be totally reversible, thus resulting in large energy losses. (iv) The elastic limit (no permanent lengthening) of uncrosslinked fibers is about 120% [11]. The α to β conversion (and initial unfolding of the γ-nodule) may be largely reversible (despite some dissipative energy) and thus explain the observed 120% elastic limit of uncrosslinked fibrin fibers. (v) Brown *et al*. [7] showed by force spectroscopy that a chain of fibrinogen monomers lengthens incrementally by about 90–100% upon the application of force. The α-helical to β-strand conversion of the coiled coils is consistent with these measurements. This conversion was also observed in computational simulations [28]. (vi) Stiffening and decreased elasticity of the fiber upon crosslinking. The role of the two αC regions in fiber assembly is still unclear; however, they are important for lateral aggregation [25–27]. The αC-connector region alone (α221–391) can extend 61 nm (122 nm for both), and the whole αC region (α221–610) can extend still farther. The αC region could, therefore, elastically connect fibrin monomers within a protofibril, and they can also easily reach across adjacent protofibrils. The αC region interactions may be partly responsible for the elastic recoil forces. It would explain that fully crosslinked fibers become stiffer, less elastic and less extensible. There are numerous crosslinking sites and full crosslinking may, thus, limit the mobility of the αC-connector. More insights into the role of the α–α and γ–γ crosslinks could be gained by extending our single fiber experiments to crosslinking mutants [24].

It should now be possible to use our data on the single fibers, and the data from our companion paper on the strength of fibrin fiber joints [29], to build a realistic, mechanical model of a blood clot, by utilizing recently developed network modeling approaches [6,9,10]. The model data could then be compared with whole clot measurements [3–5].

It would be equally interesting to build a model of a single fiber starting with an arrangement of single fibrin molecules, and test the mechanical properties of such a model against our data.

Addendum

W. Liu, C. R. Carlisle, E. A. Sparks and M. Guthold performed and designed the research; W. Liu, C. R. Carlisle and M. Guthold wrote the paper.

Acknowledgements

We thank M. C. Stahle and R. R. Hantgan for help with fluorescently labeling fibrinogen, and the NIH research resource P41 EB002025 for general support. This research was supported by: the NIH, R41 CA103120 (M. Guthold); the NSF, CMMI-0646627 (M. Guthold); and the American Heart Association, 081503E (C. R. Carlisle).

Disclosure of Conflict of Interests

The authors state that they have no conflict of interest.

Supporting Information

Additional Supporting Information may be found in the online version of this article:

Data S1. Materials and methods.
Data S2. Fibrin fiber mechanical properties.
Data S3. Partially crosslinked fibrin fiber data.
Table S1 All mechanical properties of uncrosslinked, crosslinked and partially crosslinked fibrin fibers, including generalized Kelvin model properties and data statistics.
Movie S1. Crosslinked fibrin movie.
Movie S2. Uncrosslinked fibrin movie.

Please note: Wiley-Blackwell are not responsible for the content or functionality of any supporting materials supplied by the authors. Any queries (other than missing material) should be directed to the corresponding author for the article.

References

1 Weisel JW. The mechanical properties of fibrin for basic scientists and clinicians. *Biophys Chem* 2004; **112**: 267–76.
2 Lorand L. Acquired inhibitors of fibrin stabilization: a class of hemorrhagic disorders of diverse origins. In: Green D, ed. *Anticoagulants, Physiologic, Pathologic and Pharmacologic*. Boca Raton: CRC Press, 1994: 169–91.
3 Ryan EA, Mockros LF, Weisel JW, Lorand L. Structural origins of fibrin clot rheology. *Biophys J* 1999; **77**: 2813–26.
4 Roberts WW, Lorand LL, Mockros LF. Viscoelastic properties of fibrin clots. *Biorheology* 1973; **10**: 29–42.
5 Benkherourou M, Gumery PY, Tranqui P. Quantification and macroscopic modeling of the nonlinear viscoelastic behavior of strained gels with varying fibrin concentrations. *IEEE Trans Biomed Eng* 2000; **47**: 1465–75.
6 Brown AEX, Litvinov RI, Discher DE, Purohit PK, Weisel JW. Multiscale mechanics of fibrin polymer: gel stretching with protein unfolding and loss of water. *Science* 2009; **325**: 741–4.
7 Brown AEX, Litvinov RI, Discher DE, Weisel JW. Forced unfolding of coiled-coils in fibrinogen by single-molecule AFM. *Biophys J* 2007; **92**: L30–41.

8 Kollman JM, Pandi L, Sawaya MR, Riley M, Doolittle RF. Crystal structure of human fibrinogen. *Biochemistry* 2009; **48**: 3877–86.

9 Gardel ML, Shin JH, MacKintosh FC, Mahadevan L, Matsudaira P, Weitz DA. Elastic behavior of cross-linked and bundled actin networks. *Science* 2004; **304**: 1301–5.

10 Storm C, Pastore JJ, MacKintosh FC, Lubensky TC, Janmey PA. Nonlinear elasticity in biological gels. *Nature* 2005; **435**: 191–4.

11 Liu W, Jawerth LM, Sparks EA, Falvo MR, Hantgan RR, Superfine R, Lord ST, Guthold M. Fibrin fibers have extraordinary extensibility and elasticity. *Science* 2006; **313**: 634.

12 Collet JP, Shuman H, Ledger RE, Lee ST, Weisel JW. The elasticity of an individual fibrin fiber in a clot. *Proc Natl Acad Sci USA* 2005; **102**: 9133–7.

13 Guthold M, Liu W, Stephens B, Lord ST, Hantgan RR, Erie DA, Taylor RM, Superfine R. Visualization and mechanical manipulations of individual fibrin fibers suggest that fiber cross section has fractal dimension 1.3. *Biophys J* 2004; **87**: 4226–36.

14 Carlisle CR, Coulais C, Namboothiry M, Carroll DL, Hantgan RR, Guthold M. The mechanical properties of individual, electrospun fibrinogen fibers. *Biomaterials* 2009; **30**: 1205–13.

15 Guthold M, Falvo MR, Matthews WG, Paulson S, Washburn S, Erie D, Superfine R, Brooks FP, Taylor RM. Controlled manipulation of molecular samples with the nanoManipulator. *IEEE ASME Trans Mechatron* 2000; **5**: 189–97.

16 Sader JE, Larson I, Mulvaney P, White LR. Method for the calibration of atomic-force microscope cantilevers. *Rev Sci Instrum* 1995; **66**: 3789–98.

17 Liu W, Bonin K, Guthold M. An easy and direct method for calibrating AFM lateral force measurements. *Rev Sci Instrum* 2007; **78**: 063707.

18 Silver FH, Christiansen D, Snowhill PB, Chen Y, Landis WJ. The role of mineral in the storage of elastic energy in turkey tendons. *Biomacromolecules* 2000; **1**: 180–5.

19 Guthold M, Liu W, Sparks EA, Jawerth LM, Peng L, Falvo M, Superfine R, Hantgan RR, Lord ST. A comparison of the mechanical and structural properties of fibrin fibers with other protein fibers. *Cell Biochem Biophys* 2007; **49**: 165–81.

20 Litvinov RI, Gorkun OV, Owen SF, Shuman H, Weisel JW. Polymerization of fibrin: specificity, strength, and stability of knob-hole interactions studied at the single-molecule level. *Blood* 2005; **106**: 2944–51.

21 Yang G, Cecconi C, Baase WA, Vetter IR, Breyer WA, Haack JA, Matthews BW, Dahlquist FW, Bustamante C. Solid-state synthesis and mechanical unfolding of polymers of T4 lysozyme. *PNAS* 2000; **97**: 139–44.

22 Privalov PL, Medved LV. Domains in the fibrinogen molecule. *J Mol Biol* 1982; **159**: 665–83.

23 Ryan EA, Mockros LF, Stern AM, Lorand L. Influence of a natural and a synthetic inhibitor of factor XIIIa on fibrin clot rheology. *Biophys J* 1999; **77**: 2827–36.

24 Standeven KF, Carter AM, Grant PJ, Weisel JW, Chernysh I, Masova L, Lord ST, Ariens RAS. Functional analysis of fibrin gamma-chain cross-linking by activated factor XIII: determination of a cross-linking pattern that maximizes clot stiffness. *Blood* 2007; **110**: 902–7.

25 Collet JP, Moen JL, Veklich YI, Gorkun OV, Lord ST, Montalescot G, Weisel JW. The alpha C domains of fibrinogen affect the structure of the fibrin clot, its physical properties, and its susceptibility to fibrinolysis. *Blood* 2005; **106**: 3824–30.

26 Falvo MR, Millard D, Obrien ET, Superfine R, Lord ST. Length of tandem repeats in fibrin's alpha C region correlates with fiber extensibility. *J Thromb Haemost* 2008; **6**: 1991–3.

27 Litvinov RI, Yakovlev S, Tsurupa G, Gorkun OV, Medved L, Weisel JW. Direct evidence for specific interactions of the fibrinogen alpha C-domains with the central E region and with each other. *Biochemistry* 2007; **46**: 9133–42.

28 Lim BBC, Lee EH, Sotomayor M, Schulten K. Molecular basis of fibrin clot elasticity. *Structure* 2008; **16**: 449–59.

29 Carlisle CR, Sparks EA, Der Loughian C, Guthold M. Strength and failure of fibrin fiber branch points. *J Thromb Haemost* 2010; DOI: 10.1111/j.1538-7836.2010.03824.x.